Active Osmotic Exchanger for Efficient Nanofiltration Inspired by the Kidney

Sophie Marbach and Lydéric Bocquet[*]

Laboratoire de Physique Statistique, UMR CNRS 8550, Ecole Normale Supérieure,
PSL Research University, 24 rue Lhomond, 75005 Paris, France

In this paper, we investigate the physical mechanisms underlying one of the most efficient filtration devices: the kidney. Building on a minimal model of the Henle loop—the central part of the kidney filtration—we investigate theoretically the detailed out-of-equilibrium fluxes in this separation process in order to obtain absolute theoretical bounds for its efficiency in terms of separation ability and energy consumption. We demonstrate that this separation process operates at a remarkably small energy cost as compared to traditional sieving processes while working at much smaller pressures. This unique energetic efficiency originates in the double-loop geometry of the nephron, which operates as an active osmotic exchanger. The principles for an artificial-kidney-inspired filtration device could be readily mimicked based on existing soft technologies to build compact and low-energy artificial dialytic devices. Such a "kidney on a chip" also points to new avenues for advanced water recycling, targeting, in particular, sea-water pretreatment for decontamination and hardness reduction.

Subject Areas: Fluid Dynamics

I. INTRODUCTION

Most modern processes for water recycling are based on sieving principles: A membrane with specific pore properties allows the separation of the permeating components from the retentate [1]. Selectivity requires small and properly decorated pores at the scale of the targeted molecules, and this inevitably impedes the flux and transport, making separation processes costly in terms of energy. It also raises structural challenges since high pressures are usually required to bypass the osmotic pressure. Lately, nanoscale materials—like state-of-the-art graphene, graphene oxides, or advanced membranes [2–6]—have raised hopes to boost the efficiency of separation processes. Yet, a necessary step for progress requires out-of-the-box ideas operating beyond traditional sieving separation principles.

In this context, it is interesting to investigate how biological systems are able to defy these constraints in their water cycle. They often rely on various forms of osmotically driven transport. For example, in plants, osmosis is harnessed to drive water and sugars over long distances [7,8]. As we discuss in this work, filtration processes can also benefit from osmotic transport: This is the case of the kidney.

Per day, the human kidney is capable of recycling about 200 L of water and 1.5 kg of salt, separating urea from water and salt at the low cost of 0.5 kJ/L [9] while

[*]lyderic.bocquet@lps.ens.fr

readsorbing ≈99% of the water input. The core of the kidney separation process lies in the millions of parallel filtration substructures called nephrons [9]. A striking feature is that the nephrons of all mammals present a precise loop geometry, the so-called loop of Henle. This loop plays a key role in the urinary concentrating mechanism and has been extensively studied from a biological and physiological point of view [9–17] (see also Sec. I of Ref. [18] for a short review of the physiological literature). The nephron operates the separation of urea from water near the thermodynamic limit, ∼0.2 kJ/L (see Sec. V of Ref. [18]), yet standard dialytic filtration systems, which are based on reverse osmosis and passive equilibration with a dialysate, require more than 2-orders-of-magnitude more energy [19]. Some attempts to build artificial devices mimicking the nephron were reported in the literature, but they rely on biological tissues or cell-mediated transport and cannot be easily scaled up and transferred to other separation devices [20–22]. Mimicking the separation process occurring in the kidney remains a challenge.

In this work, our goal is to take a physical perspective on the separation process at work in the nephron in order to decipher the elementary processes at work. This allows us to propose a simple biomimetic design for an osmotic exchanger inspired by the kidney's loop of Henle—see Fig. 1—combining a passive water permeation and an active salt pumping. Such an artificial counterpart can be implemented based on microfluidic elementary building blocks.

A key feature of the process is merely geometrical: The *U*-shaped loop of Henle is designed as an active osmotic exchanger, with the waste separated from water and salt via a symbiotic reabsorption. Starting with physiological

models of the nephron [12,15], we revisit the detailed out-of-equilibrium flux balance along the exchanger. Our analysis allows us to obtain, to our knowledge for the first time, absolute theoretical bounds for its efficiency in terms of separation. Furthermore, we are able to predict analytically the energetic performance of the separation process. Comparing to alternative sieving strategies like reverse osmosis and nanofiltration, we show that this osmotic exchanger operates at a remarkably small energy cost, typically 1 order of magnitude smaller than other traditional sieving processes, while working at much smaller pressures. Our predictions further assess the key role played by the second part of the loop in order to reach optimal efficiency and low energy cost.

II. TRANSPORT EQUATIONS IN AN OSMOTIC EXCHANGER

A. Geometry of an osmotic exchanger

The model we consider is sketched in Fig. 1. It is a concentrating system that possesses the same primary features as the mammalian nephron: (i) a serpentine geometry consists of (ii) a first U-loop (Henle's loop, HL) with a descending limb (D) permeable only to water—a task performed by the aquaporins in the kidney—while the second ascending limb (A) is coated with "activator" pumps—accounting for the sodium pumps in the kidney [9,23–25]; (iii) this coil is embedded in a common loose material, permeable to both water and salt, the interstitium;
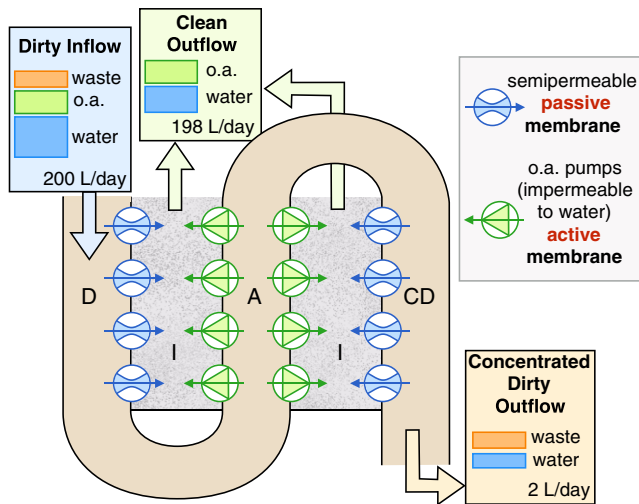

FIG. 1. The osmotic exchanger filtration system. Model for a concentrating device based on the geometry of Henle's loop in the kidney. Water, waste, and salt are carried through the loop of Henle, consisting of the descending limb (D) and ascending limb (A) and continued by the collecting duct (CD). Each limb wall allows exchanges with the interstitium (I), enabling water and salt to evacuate the loop. The remaining waste is concentrated and evacuated by the CD.

(iv) the first U-loop is continued by another loop and the so-called collecting duct (CD), again permeable to water only. This model is inspired by the so-called central core models of the nephron [12,15,26–31] (see also Sec. I of Ref. [x]). In our model though, we do not wish to accomplish a faithful description of the kidney and simplify the process to its elementary ingredients. This will also allow us to get detailed insights in the separation mechanism.

The initial solution entering the device from the D top is an aqueous solution with a waste to be extracted—in the case of the kidney, urea—with respective concentrations [Water]^{in} and [Waste]^{in}. Aside from the specific geometry of the coil, an essential feature of the process is to use an "osmotic activator"—in the case of the kidney, NaCl salt—that enters the D limb along with the mix, with concentration [Osm]^{in}. The terminology of osmotic activator is justified by the role played by the salt in this separation process, and it constitutes the main working principle of this loop: Thanks to the U-loop geometry, the pumps in the A limb generate a salinity gradient in the interstitium that passively drags, via osmosis, the water from the D limb to the interstitium. In simple words, the work performed by the ionic pumps is further harvested to also drag water osmotically in the interstitium. The geometry of the loop of Henle thus plays the role of an osmotic exchanger.

B. Transport equations and osmotic fluxes

We now quantitatively analyze the transport of the various components along the serpentine geometry sketched in Fig. 1. For the sake of simplicity, we develop a one-dimensional modelization along the tube length. The coordinate along the tube is x, and the origin is located at the top of the D limb. The length of the tube from top to first loop is L [see Fig. 2(b)]. This simplification does not alter the main ingredients. One may indeed check that the equilibration of the concentrations by diffusion processes in the orthogonal direction is fast compared to the axial velocity of the fluid, so concentrations may be considered uniform in the orthogonal direction within each limb (but they may strongly differ from limb to limb). Moreover, the velocity of the fluid in the limbs is high enough that diffusion processes along the axial direction can also be neglected. We consider, for simplicity, the steady-state regime of the system.

In the following, we first focus on the single U-loop, e.g., the loop of Henle *per se* (D + A limbs), and then extend our analysis to the complete double-loop geometry (D + A limbs +CD).

1. Descending limb

Along the D limb, the water flux evolves because of the permeation of water under the osmotic pressure across the semipermeable D limb walls. Writing the infinitesimal water balance and osmotic fluxes [32] along a slice of the D
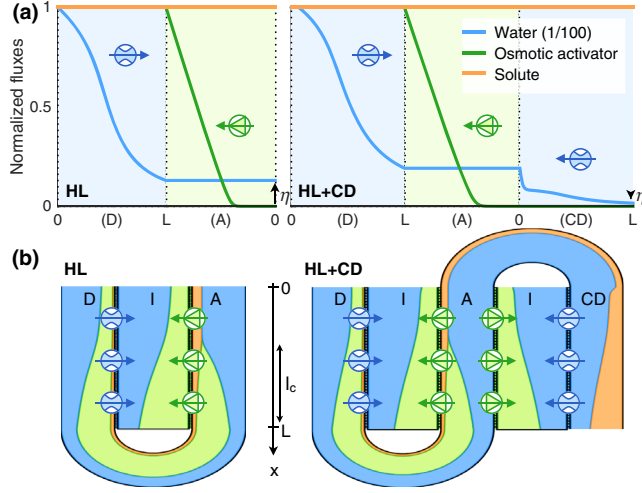
FIG. 2. Spatial distributions of the fluxes and molar fraction in the U-loop and full double loop (HL and HL $+$ CD models). (a) Fluxes of water (divided by a scaling factor of 100), osmotic activator (salt), and waste along the D and A limbs, left panel; and along the CD for the HL $+$ CD case; in this graph, the water loss ratio $\eta = q_{\text{Water}}^{\text{out}}/q_{\text{Water}}^{\text{in}}$ is the final normalized flux. (b) Spatial distribution of the molar fractions of water (divided by a scaling factor of 100), osmotic activator, and waste along the D and A limbs and in the interstitium. Note that in the (HL $+$ CD) double-loop geometry, the interstitium exchanges with all three branches (D, A, CD); although two were plotted for convenience, they have the same composition. Numerical data are calculated with parameters $L = 4.3$ mm, $P_f = 2500$ μm/s, $n = 1$.

limb allows us to write the equation for the water flux along D as

$$\frac{\partial v_D[\text{Water}]_D}{\partial x} = \frac{2P_f}{r}\ln\left(\frac{a_I^W}{a_D^W}\right), \qquad (1)$$

where v is the velocity of the fluid, P_f the permeability of the D walls, r the radius of the limb, a^W the chemical activity of water—here, assumed to be proportional to the molar fraction of water—and D (resp. I) indices refer to variables in the D (resp. the interstitium). In the D limb, all other species are conserved.

The fluid velocity can be calculated thanks to conservation of mass in every limb. For instance, in the D limb, this is written $\partial v_D/\partial x = \bar{v}_{\text{Water}}\{[(\partial[\text{Water}]_D)/\partial t]+[(\partial v_D[\text{Water}]_D)/\partial x]\}$, with $\bar{v}_{\text{Water}}$ the molar volume of water. The hydrostatic pressure drop along each limb is ruled by Poiseuille flow. However, the pressure drop is significantly small [13] and is thus neglected. Accordingly, we can safely neglect, in Eq. (1), the contribution of the hydrodynamic pressure drop to the osmotic pressure drop.

2. Ascending limb

In the A limb, the salt, denoted in the following as the osmotic activator, is actively pumped across the walls.

We consider a general case where the pumps drive n osmotic activator molecules for an elementary energy cost. In the kidney, this is provided by the dissociation energy of one adenosine triphosphate (ATP) molecule, and the stoichiometry is believed to be 3 Na$^+$ for 1 ATP [33]; Cl^- follows through the tissue walls and diffuses quickly to achieve electroneutrality [33]. We write Michaelis-Menten kinetics to describe the activator concentration evolution in the A limb [34,35]:

$$\frac{\partial v_A[\text{Osm}]_A}{\partial x} = -\frac{2nV_m}{r}\left(\frac{[\text{Osm}]_A}{K+[\text{Osm}]_A}\right)^n, \qquad (2)$$

where V_m is the maximum rate intake, K is the Michaelis constant, and A indices refer to variables associated with the A limb. The kinetics involved are assumed to be independent of the concentration of the osmotic activator in the interstitium, and furthermore, the energy requirement for the pump is assumed to be independent of the concentration of any of the constituents [33]. The kinetics described by Eq. (2) can be applied to various pumping mechanisms. All other species are conserved in the A limb. In particular, the membrane separating the A limb and the interstitium is considered to be impermeable to water.

3. Interstititum

In the interstitium, equations similar to Eq. (1) and (2) are written for the salt and water concentrations, with the sign reversed for the terms on the right-hand side. No waste is present in the interstitium. The velocity of the fluid is taken to be zero at the bottom of the interstitium.

III. RESULTS: SPATIAL DISTRIBUTIONS, FLUXES, AND OPTIMAL SEPARATION ABILITY

The previous analysis yields a set of 11 coupled and self-consistent nonlinear transport equations for the water, osmotic activator, and waste concentrations, as well as for the velocities in the various compartments. At the entrance of the device, the fluxes of water, osmotic activator (salt), and waste are prescribed as $q_{\text{Water}}^{\text{in}}$, $q_{\text{Osm}}^{\text{in}}$, and $q_{\text{Waste}}^{\text{in}}$. The integration of the previous system of equations yields the spatial distributions of the molar fractions of each component and the outcoming water and waste fluxes, $q_{\text{Water}}^{\text{out}}$ and $q_{\text{Waste}}^{\text{out}}$. The whole set of equations and boundary conditions is recalled in Sec. II of Ref. [18].

This complex system of differential equations is first solved numerically using standard methods, see Materials and Methods. Later, we also perform a systematic analysis of the transport equations at the steady state. This provides several analytical results for the spatial dependence of the concentrations and fluxes of the various components, as well as reliable estimates of the separation ability and energy cost of the system.

A typical numerical result is shown in Fig. 2 for the spatial evolution of the fluxes and molar fractions of the various components along the U-loop and double-loop geometries, at the steady state.

We now explore in detail the results in order to gain some insight on the filtration efficiency.

A. Osmotic activator pumping

We start the analysis by studying the absorption of the osmotic activator in the A limb. As highlighted in Fig. 2, what emerges from the numerical calculations is the existence of a characteristic length for reabsorption. This is confirmed by the analytical resolution of the transport equation for $[\mathrm{Osm}]_A$ and v_A in the A limb. Typically, this length scale can be constructed by balancing the input flux of the osmotic activator, $q_{\mathrm{Osm}}^{\mathrm{in}} = \pi r^2 v^{\mathrm{in}}[\mathrm{Osm}]^{\mathrm{in}}$, with the outward pumped flux, $q_{\mathrm{pump}} = 2\pi r \ell_c V_m n$ (with V_m the intake rate of the pumps), so that

$$\ell_c = \frac{q_{\mathrm{Osm}}^{\mathrm{in}}}{2\pi r V_m n}. \qquad (3)$$

This result can also be obtained from the equations by approximating the spatial derivative of the activator flux $v_A[\mathrm{Osm}]_A$ in the A limb by its value at the bottom of the loop ($x = L$) in Eq. (2). This simplified expression for ℓ_c is then obtained under the assumption that $K \sim$ 30 mmol/L $\ll [\mathrm{Osm}]^{\mathrm{in}} \simeq$ 100–200 mmol/L (Sec. III and Fig. S2 of Ref. [18]). Using typical values for the various parameters entering this equation (Ref. [18], Table 1), we find $l_c \simeq 1$ mm, which compares well to the total length of the nephron [36,37]. Beyond that length scale, the activator uptake is negligible.

Altogether, salt reabsorption occurs in a region of length ℓ_c close to the bottom of the U-loop. In the following, this allows us to split the effective domain of investigation into two different regions, where we can quantify every variable in the A limb: the deep domain, in a region of length ℓ_c close to the bottom, where osmotic activator or salt reabsorption happens on the length scale l_c; and the remaining higher domain.

A preliminary conclusion is that the length scale of salt reabsorption ℓ_c does not depend on the length of the limb L. As a result, even if L increases, salt will always be reabsorbed on the same length scale ℓ_c at the bottom of the A limb. However, the region of length $L - \ell_c$ at the top of the interstitium increases. In this region, concentrated salt coming from the bottom of the interstitium continues to be diluted by progressive water uptake under the osmotic pressure [see Fig. 2(b)].

B. Water reabsorption and optimal separation ability

With this result at hand, we can now turn to the detailed balance in water reabsorption. A key question is how much

water may be extracted with this process. We analyze both the U-loop and the double-loop geometry.

Because the velocity at the bottom of the interstitium vanishes, the osmotic activator accumulates there, increasing the osmotic pressure between the D limb and the interstitium. As a result, water is dragged out of the D limb into the interstitium. The concentration of osmotic activator in the D limb thus increases, and water leakage is possible until the osmotic pressure between the D limb and the interstitium equilibrates.

1. Maximum separation ability in the U-loop

Let us start with the investigation in the U-loop. Because the exchanges between the interstitium and the limbs are well quantified, one may express the variables of the interstitium according to the variables of the D limb (unknown so far) and the variables of the A limb (with known approximates). Accordingly, a straightforward derivation allows us to obtain two self-consistent sets of equations for the variables of the D limb alone, which can be solved, although still complex. In Ref. [18], we report the details of the analytical calculations.

Beyond the detailed solutions, some helpful analytical predictions may be extracted from these calculations. This concerns, in particular, the proportion η of water flux remaining in the tube, i.e., the water loss ratio, $\eta = q_{\mathrm{Water}}^{\mathrm{out}}/q_{\mathrm{Water}}^{\mathrm{in}}$. In Fig. 3, we plot the numerical results for η as a function of the initial osmotic activator (or salt) concentration both in the U-loop and in the double-loop geometry discussed below.

A simple yet key result can be obtained for the water loss ratio, which characterizes the separation ability. It is obtained from the analysis of Eq. (1) in the upper part of the limb, by identifying that the flux of water through the semipermeable wall should always be directed from the D limb towards the interstitium (see Sec. IV of Ref. [18] for a detailed derivation). This is written as

$$\eta = \frac{q_{\mathrm{Water}}^{\mathrm{out}}}{q_{\mathrm{Water}}^{\mathrm{in}}} \geq \eta_{\min} = \frac{[\mathrm{Waste}]^{\mathrm{in}}}{[\mathrm{Waste}]^{\mathrm{in}} + [\mathrm{Osm}]^{\mathrm{in}}}, \qquad (4)$$

where we recall that $[\mathrm{Waste}]^{\mathrm{in}}$ is the initial concentration of solute to be extracted arriving in the D limb and $[\mathrm{Osm}]^{\mathrm{in}}$ of osmotic activator.

This lower bound can be interpreted physically in terms of the osmotic pressure balance between the D limb and the interstitium. Indeed, for the water flux to be directed from D to I, the chemical balance requires that $a_I^W \leq a_D^W$ [see Eq. (1)]. This condition can be rewritten in terms of the various fluxes. On the one hand, the fluxes entering the D are $q_{\mathrm{Water}}^{\mathrm{in}}$ for water, $q_{\mathrm{Osm}}^{\mathrm{in}}$ for the osmotic activator, and $q_{\mathrm{Waste}}^{\mathrm{in}}$ for waste. On the other hand, by conservation of mass, the fluxes exiting the interstitium are $q_{\mathrm{Water}}^{\mathrm{in}} - q_{\mathrm{Water}}^{\mathrm{out}}$ for water, $q_{\mathrm{Osm}}^{\mathrm{in}}$ for the osmotic activator *if it has completely*
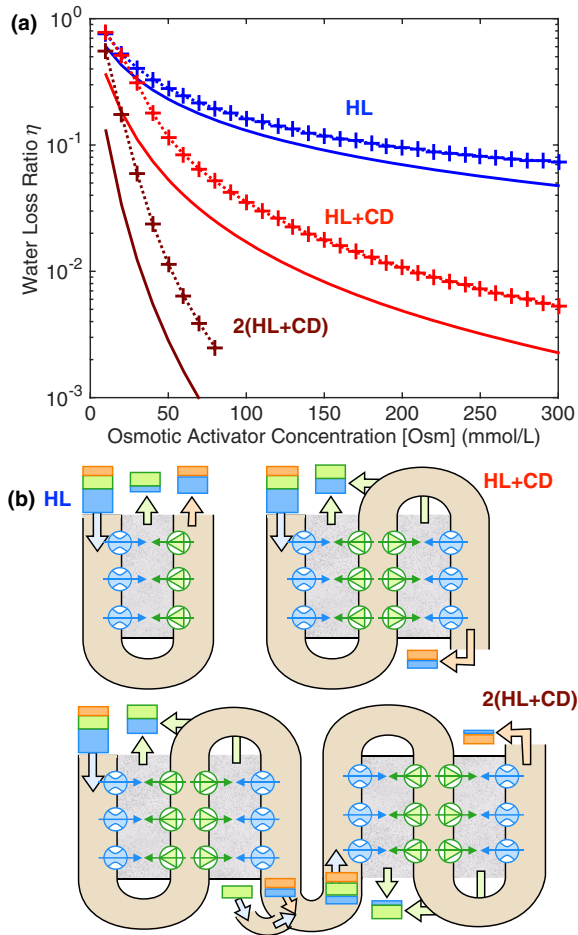
FIG. 3. Separation ability and minimal bounds. (a) Water loss ratio $\eta = q_{\text{Water}}^{\text{out}}/q_{\text{Water}}^{\text{in}}$ as a function of the initial concentration of osmotic activator $[\text{Osm}]^{\text{in}}$ (salt). Both the numerical results (crosses and dotted lines) and the predicted lower bounds (solid lines) are reported, for the single loop (HL), double-loop (HL + CD) and two double-loop cycles (2 HL + CD). The latter quantities are given by Eqs. (4) and (6) for the HL and HL + CD geometries, respectively. Numerical data are calculated with parameters $L = 4$ mm, $P_f = 2500$ μm/s, $n = 3$. (b) Schematics of the nephron-inspired systems studied in (a).

been reabsorbed, and 0 for the waste. In this minimal situation, the previous osmotic pressure balance yields

$$\frac{q_{\text{Water}}^{\text{in}} - q_{\text{Water}}^{\text{out}}}{q_{\text{Water}}^{\text{in}} - q_{\text{Water}}^{\text{out}} + q_{\text{Osm}}^{\text{in}}} \leq \frac{q_{\text{Water}}^{\text{in}}}{q_{\text{Water}}^{\text{in}} + q_{\text{Osm}}^{\text{in}} + q_{\text{Waste}}^{\text{in}}}, \quad (5)$$

and some simple algebra allows us to recover Eq. (4).

Note that it is also possible to derive an (approximate) upper analytic bound η_{max} for the water loss ratio η, by solving the equations on the species of the D in the higher and deeper parts of the limb, see Supplemental Material Sec IV.C. The upper bound η_{max} converges to the lower bound η_{min} defined by Eq. (4) in the limit of large pore permeability and/or a long tube (Supplemental Material

Fig. S3). For typical parameter values in the kidney, doubling the permeability decreases the water loss ratio by 20% and doubling the length decreases it by 60%. The lower bound on η can also be approached, i.e., $\eta_{\text{max}} \to \eta_{\text{min}}$, by allowing for a nonuniform spatial distribution of the water permeability along the D walls or of the pumps along the A walls (Supplemental Material Sec. III-C), as observed in nature. In the general case, the lower bound for η in Eq. (4) provides a good approximation for the variational dependence of η versus the initial osmotic activator (or salt) concentration, as shown in Fig. 3.

The minimal bound on the water loss ratio in Eq. (4) is a key result because it provides a fundamental measure of the separation ability of the system. To achieve a good separation of waste from water in this device, the outflux of water $q_{\text{Water}}^{\text{out}}$, including the waste, should be as small as possible; e.g., the water loss ratio η should be as small as possible. Equation (4) shows that the uncovered water η is limited by the initial molar ratio of the solute to be extracted to the one of the osmotic activator. So, no matter how efficient the activator pumps are or how high the water permeability of the membranes is, it is not possible to recycle more water from the system than $1 - \eta_{\text{min}}$.

Another way to interpret the result of Eq. (4) is to think of the osmotic exchanger as a concentrating device for the waste, i.e., any solute to be separated from water. The concentrating ability of this system, namely, $[\text{Waste}]^{\text{out}}/[\text{Waste}]^{\text{in}}$, can accordingly be expressed as a function of η as $[\text{Waste}]^{\text{out}}/[\text{Waste}]^{\text{in}} = 1/\eta$. Therefore, Eq. (4) is also a measure of the maximal concentrating ability of the system.

For typical parameter values in the kidney, the water loss ratio is $\eta \sim 0.2$ and is limited from below by $\eta_{\text{min}} \approx 0.1$ after the first U-loop of Henle. At this point, we note that such a minimal water loss ratio is still in the high range of physiological data [9]. For a human being, with $\eta \sim 0.1$ and an average flux of fluid (water, urea, and salt) through the nephrons of about 120 mL/min, the daily water loss would be tremendous, about 18 L, and accordingly not viable. This separation ability is also too low to be technologically relevant.

2. Maximum separation ability in the double loop

Remarkably, a solution to bypass this limitation has already been achieved by nature. One may indeed observe that, in addition to the U geometry of the Henle loop, the nephron exhibits a second limb: the so-called collecting duct, which is only permeable to water as the D limb (see Figs. 1–4).

A key point is that this second limb is in contact with the same interstitium, therefore allowing the reabsorption of water for a second time. From the theoretical point of view, the analysis follows the same lines as above (see Sec. VIII of Ref. [18]). The concentration of salt in the interstitium is still assumed to be well mixed or homogeneous in the
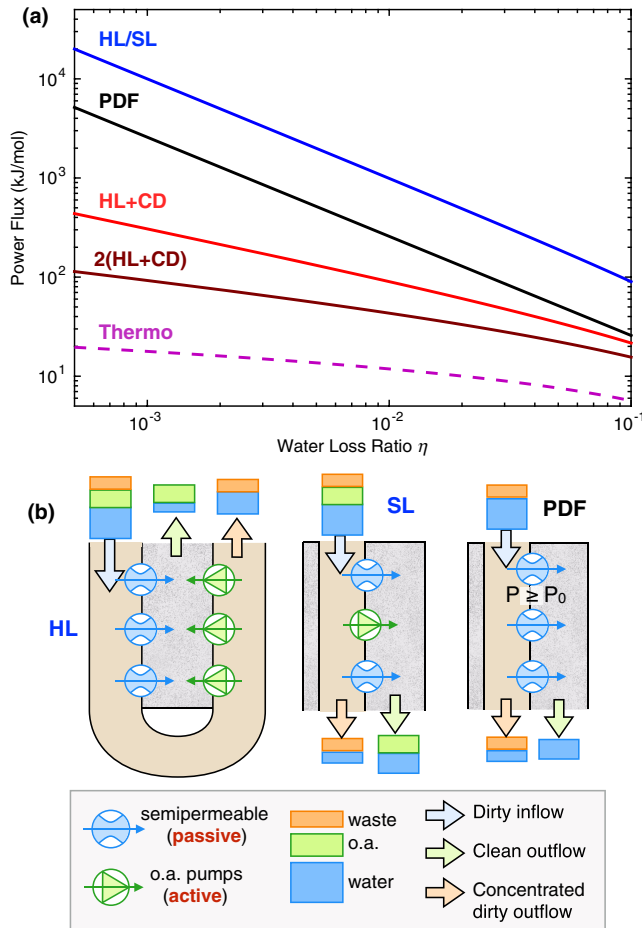
(a)

(b)

FIG. 4.   Comparison of filtration efficiencies of various systems. We show power required versus water loss ratio for the different systems. The data points are from the analytical expressions of the text. Here, $2(\text{HL} + \text{CD})$ corresponds to two successive $\text{HL} + \text{CD}$ cycles, with the addition of osmotic activator in between the two cycles. Thermo corresponds to the minimal energy required to achieve a separation defined by a given water loss ratio. The nephron working conditions correspond to $\eta \approx 0.01$. Inset: Sketch of corresponding systems. Here, HL is for a single U-loop, $\text{HL} + \text{CD}$ is a double loop, SL is a single limb, and PDF is for pressure-driven filtration. See text for detail.

orthogonal direction. Water is reabsorbed along the CD, following a permeability law similar to Eq. (1), the key difference being that the solute entering the CD has a different composition than the solute entering the D limb. A modified bound for the separation ability of the double-loop geometry is now given by

$$\eta \geq \eta_{\min}^{\text{HL}+\text{CD}} = \left[\frac{[\text{Waste}]^{\text{in}}}{[\text{Waste}]^{\text{in}} + [\text{Osm}]^{\text{in}}}\right]^2. \quad (6)$$

In Eq. (6), the square dependence, as compared to Eq. (4), originates from this second absorption step. As above, the lower bound can be reached with an adjustment of geometrical and physiological parameters of the loops.

Typically, one now finds that $\eta_{\min}^{\text{HL}+\text{CD}} \approx 0.01$, yielding a nearly 2 L daily water loss for a human being, very close to usual physiological observations [9]. This double-loop device is therefore far more efficient than the simple Henle loop, Fig. 3. As for the single U-loop, the lower bound for η in Eq. (6) provides a good approximation for the variational dependence of η versus the initial osmotic activator (or salt) concentration (see Fig. 3).

Now, putting more than two loops in series (for instance, adding a third loop with a limb covered with osmotic activator pumps) does not further improve the performance because the osmotic activator uptake only happens in the first ascending limb. However, successive cycles in the $\text{HL} + \text{CD}$ system can be done, provided that a certain amount of osmotic activator is added to the mix before each new cycle. In the case of two (respectively, N_c) successive cycles, if the concentration of the osmotic activator at the beginning of each $\text{HL} + \text{CD}$ cycle is reinitiated, the minimal water loss ratio will be that defined by Eq. (6), now squared (respectively, to the power N_c). The improvement yielded for two cycles is also plotted in Fig. 3.

Equation (6) is the first main result of this paper. In a compact formula, it summarizes how the double-loop geometry acts as an osmotic exchanger to efficiently concentrate a waste. A better waste concentration and higher water recycling ability is achieved when the osmotic activator or salt concentration is increased. Indeed, the larger the salt concentration input, the stronger the osmotic gradient in the interstitium that allows for an increased reabsorption of water. However, a higher salt concentration requires more energy to pump the salt from the A limb to the interstitium. This raises the question of the energetic performance of the HL and $\text{HL} + \text{CD}$ systems, in particular, if we want to consider them as useful working filtration devices.

IV. ENERGETIC PERFORMANCE OF THE OSMOTIC EXCHANGER

Beyond the separation ability estimate of the device, the energetic performance of the process remains to be assessed. From a physiological point of view, it is indeed vital for the kidney to operate at a minimal energy cost in view of the amount of water processed every day. Although some estimates of the free-energy expense in models of nephron have been developed, they all fail to account for the energy provided by the salt pumps [17,27,38–41]. Also, it is important to compare the energy expense of such an osmotic exchanger to more standard filtration devices.

To simplify, we assume that the permeability, pump speed, and tube length are adjusted so that η reaches its lower bound $\eta_{\min}$ in Eq. (4) or Eq. (6), depending on the geometry, respectively, U-loop or double loop.

A. Energetic cost for the single- and double-loop osmotic exchanger

In the system described in Fig. 1, the energy consumption reduces to the energy required for the pumping of the osmotic activator along the A limb. The consumed power is written as

$$\mathcal{P}_{HL} = \int_0^L \pi r^2 dx \frac{e_{ATP}}{n} N_{Osm}(x), \qquad (7)$$

with $N_{Osm}(x)$ the pumped flux of the osmotic activator across the A membrane and e_{ATP} the required energy to drive n osmotic activator molecules within a single pump, which in the case of the kidney, corresponds to that of 1 ATP molecule. Using mass conservation, $N_{Osm}(x) = -(d/dx)[v_A(x)[Osm](x)]$ and $v_A(L)[Osm]_A(L) = v_D(0)[Osm]_D(0)$, one may integrate explicitly the previous equation to obtain

$$\mathcal{P}_{HL} = q_{Osm}^{in} e_{ATP}/n \underset{\eta \to 0}{\simeq} q_{Waste}^{in} \frac{e_{ATP}/n}{\eta}. \qquad (8)$$

This is a simple and compact prediction showing that the power cost $\mathcal{P}$ diverges like the inverse of the water loss ratio η. As expected, it becomes increasingly costly to obtain a higher separation of the waste, i.e., $\eta \to 0$ [Fig. 4(b), HL].

This result describes the power consumption for the single-loop exchanger. A much better energetic efficiency is actually reached by the double-loop system, in direct line with its improved separation ability. Indeed, since the interstitium is common to the U-loop and the collecting duct, the same amount of activator pumping is harvested to reabsorb water both from the D limb and the CD. Thus, no further energetic cost is required as compared to the single U-loop. Collecting the results, one obtains

$$\mathcal{P}_{HL+CD} \underset{\eta \to 0}{\simeq} q_{Waste}^{in} \frac{e_{ATP}/n}{\sqrt{\eta}}. \qquad (9)$$

Equation (9) demonstrates that the power consumption of the double-loop system is considerably reduced compared to the single U-loop [Fig. 4(a)].

In the case of two successive cycles in the HL + CD system, with the addition of the same amount of osmotic activator to the mix before each new cycle as considered above, the energy expense is doubled—since the osmotic activator has to be readsorbed twice—but the minimal water loss ratio is squared. A two-cycle process yields a power cost $\mathcal{P}_{2\times(HL+CD)} \simeq 2q_{Waste}^{in}(e_{ATP}/n)/\eta^{1/4}$, further optimizing the energy efficiency of the process for small values of η [see Fig. 4(a)]. A N_c-cycle process would accordingly operate at a power cost $\mathcal{P}_{2\times(HL+CD)} \simeq N_c q_{Waste}^{in}(e_{ATP}/n)/\eta^{1/2N_c}$.

The above results can be compared to the minimal thermodynamic energy required for separation. The latter is estimated by computing the minimal work of separation for a given inward flux. After some algebra (see Sec. V of Ref. [18]), this can be expressed in the simple form $\mathcal{P}_{Thermo} \simeq -q_{Waste}^{in} RT \ln(\eta)$. As shown in Fig. 4(a), this result is below the previous predictions in Eqs. (8) and (9), as it should. However, increasing the number of cycles as discussed above allows us to get closer to this lower energetic bound.

Equation (9) is the second main result of this paper.

B. Power comparison to traditional sieving processes

In the context of energy efficiency, it is of utmost interest to compare the previous exchanger device with other traditional filtration or concentration systems. For this purpose, we first consider a nanofiltration (reverse-osmosis-like) system to extract the solute. This corresponds to a geometry with a single limb with water-permeable walls and acts as a pressure-driven filtration system (PDF) [see Fig. 4(b)]; no osmotic activator is required in this case. Water and waste only enter the limb at a high pressure with the same composition as in the dirty inflow in the nephron. In this situation, the hydrodynamic pressure drop is included in Eq. (1), and we similarly define the water loss ratio η as the ratio between the outward to inward flux of water through the limb (e.g., η is the ratio of water flux between the clean outflow and the dirty inflow). In this case, the high hydrostatic pressure allows us to drive water out of the descending limb, against the osmotic pressure, and concentrates waste up to a certain degree (see Sec. VII of Ref. [18] for details). If small components are also present in water—such as salt—and are also allowed to pass through the semipermeable membrane, the principle remains the same and the results are unchanged. The power required to achieve this process is proportional to the mechanical energy to drive that amount of flow with the corresponding hydrostatic pressure drop. The pressure drop may be further linked to the water loss ratio η. Some straightforward calculations along this idea, as detailed in Sec. VII of Ref. [18], allow us to predict the power required to achieve this process as

$$\mathcal{P}_{PDF} \underset{\eta \to 0}{\simeq} q_{Waste}^{in} \frac{RT}{\eta}. \qquad (10)$$

Interestingly, Eq. (10) is similar to Eq. (8) except for the thermal factor RT replacing the ATP energy, e_{ATP}/n. Quantitatively, RT is of the order of 2.5 kJ/mol, smaller than $e_{ATP}/n \simeq 10$ kJ/ mol [42]. The two behave similarly as a function of η (see Fig. 4), and the HL system and the PDF system are thus only different by a multiplicative factor. A major difference, though, is that the PDF system requires us to bypass the osmotic pressure $P > P_0 \equiv RT[Waste]^{in}$ associated with the separation of the

waste. This pressure can reach a few atmospheres depending on the concentration of the solute to extract, and such "reverse-osmosis-like" nanofiltration requires a high mechanical integrity of the material.

As an alternative geometry, we also consider a "single-limb" system corresponding to a single limb where water-permeable pores and activator pumps are intertwined on the wall of the limb [Fig. 4(a), SL]. For this device, we keep the osmotic activator in the solution. A similar analysis as for the single U-loop shows that the single-limb system is basically equivalent to the HL [see Fig. 4(b) and Sec. VI of Ref. [18]].

Altogether, Fig. 4 demonstrates that the double-loop exchanger, with one or more cycles, outperforms traditional filtration systems in terms of power efficiency while working at small pressure.

V. DISCUSSION

These results show that with the double-loop geometry of the collecting duct in series with the Henle loop, nature has evolved towards a most efficient geometry to filter out urea. From a technological point of view, it would therefore be highly inspiring to reproduce such a filtration device. This requires both the specific double-loop geometry highlighted above and the use of an osmotic activator in the solution. We argue that all required ingredients are at our disposal to fabricate such an artificial nephron. Semipermeable membranes will play the role of water-permeable D and CD walls, replacing aquaporin-coated membranes. For salt used as an osmotic activator, the ion pump functionality can be mimicked using a stack of ion-selective membranes, with an electric field as the driving force, similar in spirit to electrodialytic processes [43]. Note that any ionic species is, in general, a good candidate for an osmotic activator, for it can be easily manipulated with electric fields—although monovalent species should be used to begin with. Altogether, modern microfabrication technologies developed for microfluidics would allow us to directly mimic the setup in Fig. 1 [44,45], with several devices possibly working in parallel (for more details, we suggest a detailed implementation of the device in Sec. IX of Ref. [18]).

From the point of view of transport, such an artificial device can be described by the very same equations as above, Eqs. (1)–(4). The pumping energy is replaced by the electric power required to displace the ions, which is written as $e = \mathcal{F}\Delta\mathcal{V}/2$ for pumping under a voltage drop $\Delta\mathcal{V}$ across the ion-selective membranes and replacing e_{ATP}/n. The power consumption thus takes an expression similar to Eq. (9):

$$\mathcal{P}_{\text{elec}} \underset{\eta \to 0}{\simeq} q_{\text{Waste}}^{\text{in}} \frac{\mathcal{F}\Delta\mathcal{V}/2}{\sqrt{\eta}}, \tag{11}$$

now with $\mathcal{F}\Delta\mathcal{V}/2 \simeq 5\text{–}50$ kJ/mol (using a value of $\Delta\mathcal{V} \simeq 0.1\text{–}1$ V [43]).

Altogether, mimicking an osmotic exchanger would allow the development of novel filtration devices and dialytic systems. A "kidney on a chip" constitutes a paradigm change as compared to actual dialytic systems involving a standard sieving process, which are difficult to miniaturize [46]: This allows for a compact design, with low energy consumption. Because of its low working pressure, this also allows us to use soft materials in its design.

Such systems could also be used advantageously in the pretreatment stage of standard desalination processes. Pretreatment to separate the basic contaminants from salty water [1] typically costs more than 1 kJ/L in reverse-osmosis plants [47,48]. Contrary to standard electrodialysis, one key point of the kidney on a chip is that the extraction of ions is done from the brine. Using recent progress on ion selective membranes (e.g., monovalent selective) [49–51], the kidney-on-a-chip geometry could effectively provide decontamination and dionization of targeted heavy ions and significantly diminish water hardness. This would reduce the corresponding energy cost and considerably improve the global energetic efficiency of the desalination process.

More inspiration could certainly be drawn from the kidney. For instance, the ionic pumps responsible for sodium reabsorption in the ascending limb are able to discriminate between sodium and potassium ions [33]. So far, only nature has succeeded in making such a monovalent specific membrane.

[1] M. Elimelech and W. A. Phillip, *The Future of Seawater Desalination: Energy, Technology, and the Environment*, Science **333**, 712 (2011).

[2] T. Humplik, J. Lee, S. C. O'Hern, B. A. Fellman, M. A. Baig, S. F. Hassan, M. A. Atieh, F. Rahman, T. Laoui, R. Karnik, and E. N. Wang, *Nanostructured Materials for Water Desalination*, Nanotechnology **22**, 292001 (2011).

[3] M. Heranian, A. B. Farimani, and N. R. Aluru, *Water Desalination with a Single-Layer* MoS$_2$ *Nanopore*, Nat. Commun. **6**, 8616 (2015).

[4] J. K. Holt, Hyung G. Park, Y. Wang, M. Stadermann, A. B. Artyukhin, C. P. Grigoropoulos, A. Noy, and O. Bakajin, *Fast Mass Transport through Sub-2-Nanometer Carbon Nano-tubes*, Science **312**, 1034 (2006).

[5] R. K. Joshi, P. Carbone, F. C. Wang, V. G. Kravets, Y. Su, I. V. Grigorieva, H. A. Wu, A. K. Geim, and R. R. Nair, *Precise and Ultrafast Molecular Sieving through Graphene Oxide Membranes*, Science **343**, 752 (2014).

[6] A. Siria, P. Poncharal, A.-L. Biance, Rmy Fulcrand, X. Blase, S. T. Purcell, and L. Bocquet, *Giant Osmotic Energy Conversion Measured in a Single Transmembrane Boron Nitride Nanotube*, Nature (London) **494**, 455 (2013).

[7] K. H. Jensen, E. Rio, R. Hansen, C. Clanet, and T. Bohr, *Osmotically Driven Pipe Flows and Their Relation to Sugar Transport in Plants*, J. Fluid Mech. **636**, 371 (2009).

[8] S. M. Henton, *Revisiting the Münch pressure–Flow Hypothesis for Long-Distance Transport of Carbohydrates: Modelling the Dynamics of Solute Transport Inside a Semipermeable Tube*, J. Exp. Bot. **53**, 1411 (2002).

[9] R. Greger and U. Windhorst, *Comprehensive Human Physiology: From Cellular Mechanisms to Integration* (Springer-Verlag, Berlin, 1996).

[10] C. W. Gottschalk and M. Mylle, *Evidence that the Mammalian Nephron Functions as a Countercurrent Multiplier System*, Science **128**, 594 (1958).

[11] L. Bankir, N. Bouby, and M. M. Trinh-Trang-Tan, *2 The Role of The Kidney in the Maintenance of Water Balance*, Baillière's Clinical Endocrinology and Metabolism **3**, 249 (1989).

[12] J. L. Stephenson, *Concentration of Urine in a Central Core Model of the Renal Counterflow System*, Kidney international **2**, 85 (1972).

[13] P. J. Palatt and G. M. Saidel, *Countercurrent Exchange in the Inner Renal Medulla: Vasa Recta-descending Limb System*, Bull. Math. Biol. **35**, 431 (1973).

[14] S. R. Thomas, *Inner Medullary Lactate Production and Accumulation: A Vasa Recta Model*, Am. J. Physiol. Renal Physiol. **279**, F468 (2000).

[15] D. Foster, J. A. Jacquez, and E. Daniels, *Solute Concentration in the Kidney-II. Input-Output Studies on a Central Core Model*, Math. Biosci. **32**, 337 (1976).

[16] A. T. Layton, *A Mathematical Model of the Urine Concentrating Mechanism in the Rat Renal Medulla. I. Formulation and Base-Case Results*, Am. J. Physiol. Renal Physiol. **300**, F356 (2010).

[17] A. Edwards, *Modeling Transport in the Kidney: Investigating Function and Dysfunction*, Am. J. Physiol. Renal Physiol. **298**, F475 (2010).

[18] See Supplemental material at http://link.aps.org/supplemental/10.1103/PhysRevX.6.031008 for details on analytical derivations and computations.

[19] Phoenix X 36 brochure (Gambro, 2009), https://www.baxter.com/assets/downloads/products_expertise/renal_therapies/Phoenix_X36_Hemodialysis_System.pdf.

[20] J. Borenstein, E. Weinberg, B. Orrick, C. Sundback, M. Kaazempur-Mofrad, and J. Vacanti, *Microfabrication of Three-Dimensional Engineered Scaffolds*, Tissue Eng. Part A **13**, 1837 (2007).

[21] J. Kim, F. Garzotto, F. Nalesso, D. Cruz, J. Kim, E. Kang, H. Kim, and C. Ronco, *A Wearable Artificial Kidney: Technical Requirements and Potential Solutions*, Expert Rev. Med. Dev. **8**, 567 (2011).

[22] P. Armignaco, F. Garzotto, M. Neri, A. Lorenzin, and C. Ronco, *Wak Engineering Evolution*, Blood purification **39**, 110 (2015).

[23] C.-L. Chou, M. A. Knepper, A. N. Hoek, D. Brown, B. Yang, T. Ma, and A. S. Verkman, *Reduced Water Permeability and Altered Ultrastructure in Thin Descending Limb of Henle in Aquaporin-1 Null Mice*, J. Clin. Invest. **103**, 491 (1999).

[24] S. Nielsen, J. Frkiaer, D. Marples, T. H. Kwon, P. Agre, and M. A. Knepper, *Aquaporins in the Kidney: From Molecules to Medicine*, Physiol. Rev. **82**, 205 (2002).

[25] R. Greger and E. Schlatter, *Presence of Luminal k+, a Prerequisite for Active NaCl Transport in the Cortical Thick Ascending Limb of Henle's Loop of Rabbit Kidney*, Pflügers Arch. **392**, 92 (1981).

[26] J. A. Jacquez, D. Foster, and E. Daniels, *Solute Concentration in the Kidney—I. A Model of the Renal Medulla and Its Limit Cases*, Math. Biosci. **32**, 307 (1976).

[27] J. Stephenson, *Concentration Engines and the Kidney: I. Central Core Model of the Renal Medulla*, Biophys. J. **13**, 512 (1973).

[28] J. Stephenson, *Concentration Engines and the Kidney: II. Multisolute Central Core Systems*, Biophys. J. **13**, 546 (1973).

[29] J. Stephenson, *Concentration Engines and the Kidney: III. Canonical Mass Balance Equation for Multinephron Models of the Renal Medulla*, Biophys. J. **16**, 1273 (1976).

[30] J. Stephenson, R. Tewarson, and R. Mejia, *Quantitative Analysis of Mass and Energy Balance in Non-ideal Models of the Renal Counterflow System*, Proc. Natl. Acad. Sci. U.S.A. **71**, 1618 (1974).

[31] J. Stephenson, *Models of the Urinary Concentrating Mechanism*, Kidney international **31**, 648 (1987).

[32] A. Finkelstein, *Water Movement through Lipid Bilayers, Pores, and Plasma Membranes* (John Wiley & Sons, NewYork, 1987).

[33] R. Greger and E. Schlatter, *Properties of the Basolateral Membrane of the Cortical Thick Ascending Limb of Henle's Loop of Rabbit Kidney*, Pflügers Arch. **396**, 325 (1983).

[34] B. Yang and J. M. Sands, *Urea Transporters* (Springer Science+ Business Media, Dordrecht, 2014).

[35] R. P. Garay and P. J. Garrahan, *The Interaction of Sodium and Potassium with the Sodium Pump in Red Cells*, J. Physiol. **231**, 297 (1973).

[36] M. A. Knepper, R. A. Danielson, G. M. Saidel, and R. S. Post, *Quantitative Analysis of Renal Medullary Anatomy in Rats and Rabbits*, Kidney international **12**, 313 (1977).

[37] H. Koepsell, W. Kriz, and J. Schnermann, *Pattern of Luminal Diameter Changes along the Descending and Ascending Thin Limbs of the Loop of Henle in the Inner Medullary Zone of the Rat Kidney*, Z. Anat. Entwickl.-Gesch. **138**, 321 (1972).

[38] J. Newburgh, *The Changes which Alter Renal Osmotic Work*, J. Clin. Invest. **22**, 439 (1943).

[39] A. Layton, *Mathematical Modeling of Kidney Transport*, Wiley Interdiscip. Rev.: Syst. Biol. Med. **5**, 557 (2013).

[40] B. Hargitay and W. Kuhn, *The Multiplication Principle as the Basis for Concentrating Urine in the Kidney*, J. Am. Soc. Nephrol. **12**, 1566 (2001); Reprinted from Chemie **55**, 539 (1951).

[41] S. Hervy and S. R Thomas, *Inner Medullary Lactate Production and Urine-Concentrating Mechanism: A Flat Medullary Model*, Am. J. Physiol. Renal Physiol. **284**, F65 (2003).

[42] B. Alberts, J. Lewis, M. Raff, K. Roberts, and P. Walter, *Molecular Biology of the Cell*, 4th ed. (Garland-Science, New York, 2002).

[43] J. W. Post, J. Veerman, H. V. M. Hamelers, G. J. W. Euverink, S. J. Metz, Kitty Nymeijer, and C. J. N. Buisman, *Salinity-Gradient Power: Evaluation of Pressure-Retarded Osmosis and Reverse Electrodialysis*, J. Membr. Sci. **288**, 218 (2007).

[44] B. B. Sales, M. Saakes, J. W. Post, C. J. N. Buisman, P. M. Biesheuvel, and H. V. M. Hamelers, *Direct Power Production from a Water Salinity Difference in a Membrane-Modified Supercapacitor Flow Cell*, Environ. Sci. Technol. **44**, 5661 (2010).

[45] J. de Jong, R. G. H. Lammerink, and M. Wessling, *Membranes and Microfluidics: A Review*, Lab Chip **6**, 1125 (2006).

[46] W. H. Fissell, H. D. Humes, A. J. Fleischman, and S. Roy, *Dialysis and Nanotechnology: Now, 10 Years, or Never?*, Blood purification **25**, 12 (2007).

[47] R. Semiat, *Energy Issues in Desalination Processes*, Environ. Sci. Technol. **42**, 8193 (2008).

[48] C. Fritzmann, J. Löwenberg, T. Wintgens, and T. Melin, *State-of-the-Art Reverse Osmosis Desalination*, Desalination **216**, 1 (2007).

[49] R. K. Nagarale, G. S. Gohil, and V. K. Shahi, *Recent Developments on On-Exchange Membranes and Electromembrane Processes.*, Adv. Colloid Interface Sci. **119**, 97 (2006).

[50] J. Li, M.-I. Zhou, J.-y. Lin, W.-y. Ye, Y.-q. Xu, J.-n. Shen, C.-j. Gao, and B. Van der Bruggen, *Mono-valent Cation Selective Membranes for Electrodialysis by Introducing Polyquaternium-7 in a Commercial Cation Exchange Membrane*, J. Membr. Sci. **486**, 89 (2015).

[51] S. C. O'Hern, M. S. H. Boutilier, J.-C. Idrobo, Y. Song, J. Kong, T. Laoui, M. Atieh, and R. Karnik, *Selective Ionic Transport through Tunable Subnanometer Pores in Single-Layer Graphene Membranes*, Nano Lett. **14**, 1234 (2014).